

## Electron scattering in a multiwall carbon nanotube bend junction studied by scanning tunneling microscopy

L. Tapasztó,<sup>1,\*</sup> P. Nemes-Incze,<sup>2</sup> Z. Osváth,<sup>1</sup> Al. Darabont,<sup>2</sup> Ph. Lambin,<sup>3</sup> and L. P. Biró<sup>1</sup>

<sup>1</sup>Research Institute for Technical Physics and Materials Science, H-1525 Budapest, P.O. Box 49, Hungary

<sup>2</sup>Faculty of Physics, “Babes-Bolyai” University, Str M. Kogalniceanu No 1, R-3400 Cluj-Napoca, Romania

<sup>3</sup>Facultes Universitaire Notre Dame de la Paix, 61 Rue de Bruxelles, B-5000 Namur, Belgium

(Received 16 December 2005; revised manuscript received 7 October 2006; published 13 December 2006)

The atomic resolution scanning tunneling microscopy investigation of a multiwall carbon nanotube bend junction is reported. Atomic resolution images taken at the junction region revealed position-dependent modulation of the electronic density of states, with a period larger than but commensurate to the underlying atomic lattice, attributed to the scattering of electrons on defect sites present in the junction region. We propose an interference model, suitable to interpret the experimentally observed electron density patterns by considering electronic states near the bands crossing points involved in the scattering processes. The model predicts that complex charge density oscillations present near defects are tunable by varying the applied bias potential.

DOI: [10.1103/PhysRevB.74.235422](https://doi.org/10.1103/PhysRevB.74.235422)

PACS number(s): 73.22.-f, 73.63.Fg

### I. INTRODUCTION

The unique relationship between the atomic structure and electronic properties of carbon nanotubes has been the focus of attention since their discovery.<sup>1,2</sup> The presence of defects in nanostructured materials is expected to substantially alter their electronic behavior. Often the modifications, induced by native or artificially created defects, confer on the nanotubes the necessary functionality for realization of different types of electronic devices; a carbon nanotube bend junction is an eloquent example of such a device.<sup>3-5</sup> Transport measurements on carbon nanotubes containing defects indicate that the defect sites not only act as scattering centers for electrons but also behave as gate tunable barriers.<sup>6,7</sup> This specific behavior has its origins in the quantum coherence phenomena, leading to Fermi energy-dependent, long-range interference effects.<sup>6,8,9</sup>

Scanning tunneling microscopy (STM) is a method that can directly reveal interference patterns in the electron density distribution of solid surfaces. Such interference patterns, known as Friedel oscillations present near different types of defects, were observed by STM on both metal<sup>10</sup> and doped semiconductor<sup>11</sup> surfaces. On graphite surfaces, similar oscillations are known as  $\sqrt{3}$ -type superstructures<sup>12</sup> due to the special correlation between the oscillations and the underlying atomic structure of the hexagonal lattice.

Electron-wave interference patterns were also observed by STM on single-walled carbon nanotubes (SWCNTs) containing defect sites<sup>9,13</sup> near tube caps<sup>14</sup> and intramolecular junctions joining nanotubes with different helicities.<sup>15</sup> The phenomenon was applied to directly probe the one-dimensional (1D) energy band dispersion near the Fermi level in metallic SWCNTs.<sup>9</sup> Recently  $\sqrt{3}$ -type superstructures have been observed by STM measurements on ion-irradiated multiwalled carbon nanotubes (MWCNTs).<sup>16</sup>

Two kinds of effects induced by the presence of the defects in carbon nanotubes (CNTs) directly perceptible by STM measurements have been revealed:

(1) Short-range ( $\sim 1$  nm) modifications in the local density of states (LDOS) at the defect site are due to localized

states and can be directly related to the atomic structure of the defect. They manifest themselves as hillocklike protrusions in STM images.

(2) Beside these very local modifications, defects also mediate a redistribution of electron density on a larger scale, which is primarily determined by the available scattered electron states.<sup>17,18</sup> These long-range effects appear as superstructure patterns in STM images.

Mizes and Foster<sup>19</sup> demonstrated theoretically that electronic superstructures observed by STM on graphite are indeed the consequence of the interference between electron waves scattered by defects and those characterized by regular electron wave functions of graphite.

In order to describe the long-range interference effects, a simple but effective interference model was constructed by Shedd and Russell,<sup>20</sup> suitable to reproduce the experimentally observed superstructure patterns. Their results were confirmed by tight binding<sup>18</sup> and first-principles<sup>21</sup> calculations and applied successfully in interpretation of various experimental results,<sup>18,22</sup> being able to describe most of the simple superstructure patterns observed experimentally. However, experiments often reveal more complex patterns of coexisting superstructures.<sup>12,17,20</sup>

STM is well known for its ability to image individual wave functions of CNTs.<sup>23,24</sup> In this paper we report on how STM can be used to collect information, through long-range interference effects, about the defect-scattered electronic states which can seriously affect the transport characteristics of the defective carbon nanotubes. We show that STM images of coexisting superstructures are signatures of coherent scattering of electrons by defects, between the few electron states available in CNTs in the vicinity of bands crossing points ( $K$  points of the Brillouin zone). Fermi energy-dependent scattering of electrons in nanotubes is also discussed. We believe that the detailed understanding of defect-induced long-range modifications on electronic behavior of nanotubes is essential in the development of novel molecular electronic devices based on carbon nanotubes.

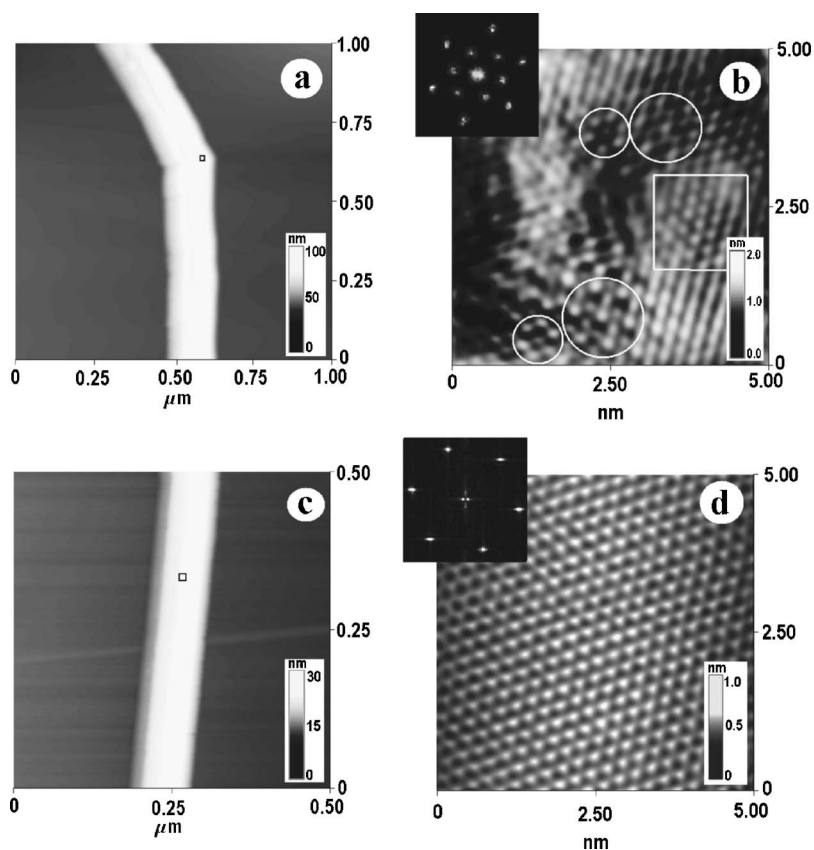


FIG. 1. (a) STM image of a multiwalled carbon nanotube bend junction with a bend angle of  $30^\circ$ . (b) Atomic resolution achieved in the junction region showing complex interference patterns of coexisting superstructures. For the sake of comparison the atomic resolution image (d) of a defect-free MWCNT (c) is also presented. 2D Fourier transforms of current images are shown as insets of the atomic resolution images recorded at 0.1 V bias.

## II. EXPERIMENTAL

The MWCNTs investigated by scanning tunneling microscopy were produced by an injection spray pyrolysis chemical vapor deposition (CVD) method involving the pyrolysis of a ferrocene-xylene precursor at relatively low temperatures ( $\sim 800^\circ\text{C}$ ). The synthesis processes were carried out in Ar atmosphere at 60 ml/h active solution flow rate. A detailed description of the experimental setup and synthesis process is given in Ref. 25.

In order to become suitable for STM measurements, 1 mg of the as-grown nanotube sample was ultrasonicated in ethanol for 1 h; then droplets of the suspension were dispersed on freshly cleaved highly oriented pyrolytic graphite (HOPG) substrate.

The STM measurements were carried out at ambient conditions in constant current mode with tunneling currents of 0.2–1 nA and bias voltages ranging from 50 mV to 1 V. Atomic resolution images were typically achieved with the current set to 1 nA and 0.1 V bias.

## III. RESULTS AND DISCUSSION

Figure 1(a) presents the STM image of an as-grown MWCNT bend junction with an apparent height of 40 nm and a bend angle of  $30^\circ$ . It is well known that due to the relatively low growth temperatures (characteristic to CVD methods), native topological defects often occur in the structure of CVD-grown nanotubes.<sup>26</sup> These structural defects were identified to be most probably pentagon-heptagon pairs located at the junction region.<sup>15</sup> Specific configurations of

the defects may lead to formation of nanotube bend junctions.<sup>27</sup> However, in the case of the investigated MWCNT bend junction we were not able to identify the localized states which could have been directly related to the precise position of the defects.<sup>15</sup> This might be due to the geometrical location of the defect which was not directly accessible for the STM measurement, for example, a bend junction containing pentagons and heptagons at the lateral sites of the junction since STM can access only the top part of the nanotube and these defect states have a very local character.

However, the atomic resolution images achieved at the junction region (indicated by the small rectangle in Fig. 1(a)), revealed a modulation of the electron density distribution with a period larger than, but commensurate to, the underlying atomic lattice of the multiwalled nanotube [Fig. 1(b)]. The patterns formed by the redistribution of the electronic density in the junction region closely resemble the most commonly observed  $\sqrt{3}$ -type electronic superstructures of graphite occurring near defect sites.<sup>20</sup> The observed patterns correspond to the case of simple constructive and destructive interference patterns<sup>20</sup> marked by large respectively smaller circles in Fig. 1(b). However these patterns, complementary from the interference point of view, occur side by side in the atomic resolution image of the junction, which cannot be interpreted in the framework of the available interference models.<sup>12,18,20</sup> Similar position-dependent long-range interference patterns have been observed in several experiments on graphite surfaces, i.e., near Pt particles,<sup>12</sup> Au clusters,<sup>20</sup> chemisorbed hydrogen, and atomic vacancies induced by a hydrogen-plasma treatment,<sup>17,18</sup> but to our knowledge this is

the first time that they are revealed on CNTs.

For the sake of comparison, atomic resolution achieved on the defect-free region of a straight MWCNT is presented in Fig. 1(d). The triangular lattice of graphite is revealed, which indicates that the two outermost graphene layers exhibit *ABAB* stacking, in agreement with previous experimental findings on large-diameter MWCNT<sup>16,28</sup> and carbon fibers subjected to heat treatment.<sup>29</sup>

The two-dimensional (2D) Fourier transforms of the current images are shown as insets of the atomic resolution images. In the Fourier transform of the STM image taken at the junction, new peaks appear at smaller wave vectors as compared to the 2D Fourier image of the defect-free nanotube. The additional peaks form a smaller hexagon corresponding to the corners of the first Brillouin zone (BZ) of the hexagonal lattice, which is also a typical signature of  $\sqrt{3}$ -type superstructures in hexagonal lattices.<sup>17,18</sup>

STM images recorded at low bias voltages, with a good approximation, map the square modulus of the wave functions of the electron states near the Fermi surface.<sup>30</sup> The individual wave functions of metallic carbon nanotubes near the Fermi level were calculated theoretically<sup>31</sup> and then identified experimentally by scanning tunneling spectroscopy measurements.<sup>23</sup> We propose that the origin of the experimentally observed superstructures (electron density oscillations) is the interference of the regular electron wave functions of CNTs and those coherently scattered by the structural defects present in the junction region.

Due to large electron coherence lengths in CNTs,<sup>32</sup> the superposition of regular and defect-scattered wave functions may induce long-range spatial modulation of the electron density<sup>9</sup> directly perceptible by STM, even at several-nanometer distances from the defect sites.

Two different coherent backscattering mechanisms were identified for electrons at the Fermi surface in carbon nanotubes<sup>31</sup> [Fig. 2(a) and 2(b)]:

(1) Small momentum scattering is possible via the coupling between bands crossing with opposite slopes at  $K$  and  $K'$  points of the BZ. When the Fermi surface exactly coincides with the  $K$  points, the forward-traveling and backward-scattered wave vectors are equal and the lattice periodicity of the electron density distribution is conserved. Hence, no detectable signature in STM images is expected for this kind of scattering (unless the rotational symmetry of the STM image is broken<sup>31</sup>).

(2) Large momentum scattering takes place between two nonequivalent  $K$  points of the Fermi surface. This mechanism corresponds to a momentum change of  $\mathbf{q} = 2\mathbf{k}_F = \mathbf{k}_F'$  [Fig. 2(b)], respectively, a modulation of  $\lambda_F$  wavelength in direct space electron density distribution which appears as a homogeneous  $\sqrt{3}$ -type superstructure in STM images.<sup>13,18</sup>

The above-mentioned scattering mechanisms hold, in particular, for the electronic states located exactly at the  $K$  points of the Brillouin zone, i.e., at zero applied bias potential ( $V=0$ ) and no Fermi level shift ( $\delta E_F=0$ ).

In order to be able to interpret position-dependent superstructure patterns, we propose a model which also considers states slightly away from the  $K$  points to be involved in the scattering process. This situation happens in practice when we apply a finite bias voltage between the STM tip and the

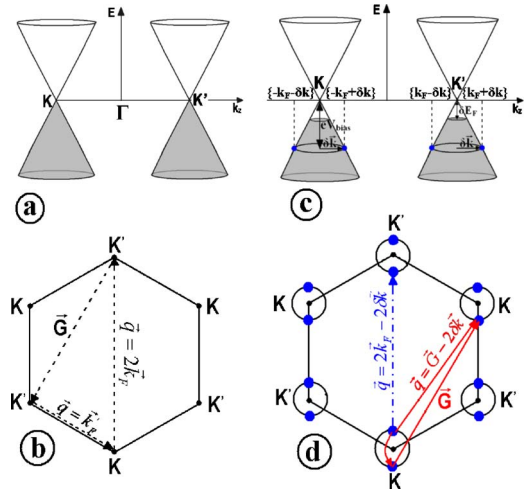


FIG. 2. (Color online) Dispersion of the states near two non-equivalent  $K$  points of the BZ. (a) For an isolated armchair tube ( $V=0$ ;  $\delta E_F=0$ ) the electronic states involved in the tunneling process are located at the Fermi surface which coincides with the  $K$  points. (b) Large momentum backscattering of electrons at the  $K$  point leading to homogenous  $\sqrt{3}$ -type superstructures. (c) At finite bias potential or shifted Fermi level ( $V \neq 0$  or  $\delta E_F \neq 0$ ), electronic states away from  $K$  points get involved in the tunneling process. (d) Possible backscattering mechanisms of electrons for states away from the  $K$  points.

sample, in which case the Fermi levels of the electrodes are shifted relatively to each other, allowing states away from the  $K$  points to contribute to the tunnel current, or when the Fermi level of the nanotube itself is shifted away from the  $K$  points.

As a simple example to illustrate the process, we consider a metallic armchair nanotube [Fig. 2(c)].

In real tunneling experiments a small but finite bias voltage is applied between the sample and STM tip in order to make a tunneling direction preferential and a net electronic current measurable. The applied bias potential shifts the relative position of the Fermi energies of the two electrodes, allowing electronic states away from the  $K$  points to contribute to the tunnel current.

There are also several possible mechanisms which may lead to the shift of the Fermi level of the nanotube itself, i.e., doping of the nanotube from the substrate,<sup>33</sup> chemical doping,<sup>34</sup> electrostatic doping,<sup>35</sup> or charging of the nanotube due to the applied bias voltage.<sup>36</sup>

In our case a Fermi-level shift might occur due to the charging of the tube due to the applied bias potential. The STM images in our experiments were recorded with the bias potential applied to the sample (i.e., the HOPG substrate). In standard STM measurement configurations the tube-support junction is expected to have a much larger transmittance than the tube-tip tunnel junction, which may lead to the charging of the nanotube due to the asymmetry between the electron injecting and collecting couplings.<sup>36,37</sup> In this case a Fermi-level shift  $\delta E_F = E_F - E_F' = \alpha V$  proportional with the applied bias voltage  $V$  may occur.

As illustrated in Fig. 2(c), for the electronic states away from the  $K$  points the forward and backward propagating

modes of the nanotube are no longer characterized by wave vectors of equal magnitude,

$$|\delta\vec{k}(E)| = \frac{2\delta E}{3\gamma_0 a_{C-C}}, \quad (1)$$

where  $\delta E$  is the distance of energy levels relative to band crossing points,  $\gamma_0$  is the nearest-neighbor C-C energy overlap integral, and  $a_{C-C}$  is the nearest-neighbor distance between C atoms.

This in turn implies some important consequences on the electronic behavior of the nanotube. Small momentum scattering will no longer conserve the lattice periodicity due to the presence of a momentum change of  $\mathbf{q}=2\delta\mathbf{k}$ . Experimental evidence of such kind of scattering is provided by Liang *et al.*<sup>38</sup> Also, large momentum scattering processes with momentum changes different from  $2\mathbf{k}_F$  become possible due to the new states involved in the tunneling process.

Therefore the spatial distribution of electron density imaged by STM results from the superposition of the few regular states of the nanotube<sup>23</sup> available near the  $K$  and  $K'$  points plus the wave functions of the states coherently scattered by the defect site present in the junction region, including both large and small momentum scattering processes. In order to be consistent with a general case including the shift of the Fermi level, we have to sum all the states with energies between the shifted Fermi energy  $E'_F = E_F - \delta E_F$  and the applied bias potential.

$$\begin{aligned} \Psi(\vec{r}) = & \int_{E_F - eV}^{E'_F} dE \sum_{\{\vec{k}_F^j\}} \phi_j e^{i[\vec{k}_F^j \pm \delta\vec{k}_Z(E)]\vec{r}} + R_j^S e^{i[\vec{k}_F^j \mp \delta\vec{k}_Z(E)]\vec{r}} \\ & + R_j^L e^{-i[\vec{k}_F^j \pm \delta\vec{k}_Z(E)]\vec{r}} \end{aligned} \quad (2)$$

where

$$\begin{aligned} \vec{k}_F^j = & \vec{k}_Z^j + \vec{k}_\perp^j; \quad |\vec{k}_\perp^j| = \frac{2}{d_{tube}} \left( n - \frac{\nu}{3} \right) \\ n = & 0, 1, 2, \dots; \quad \nu = 0, \pm 1; \quad \text{and } |\delta\vec{k}(E)| = \frac{2|E_F - E|}{3\gamma_0 a_{C-C}}. \end{aligned}$$

The first term of the sum in Eq. (2) gives the wave functions of the defect-free nanotube.<sup>23</sup> The  $R_j^S$  and  $R_j^L$  coefficients are complex amplitudes representing the contribution of different scattered states due to small- and large-momentum scattering, respectively. These reflection amplitudes can be related to the off-diagonal elements of the  $\rho_{\alpha\beta} = \langle \psi_\alpha^* \delta(E-H) \psi_\beta \rangle$  density matrix in the formalism used by Kane and Mele,<sup>31</sup> and their values explicitly depend on the detailed structure of the scatterer.  $\vec{k}_z^j$  and  $\vec{k}_\perp^j$  are the axial and perpendicular components of the Fermi wave vectors, respectively, while  $d_{tube}$  denotes the diameter of the nanotube.

In order to reproduce a particular experimentally observed electron density distribution, we have to adjust the  $\alpha$ ,  $\phi_j$ ,  $R_j^S$ , and  $R_j^L$  coefficients in Eq. (2).

By fitting the reflection amplitudes  $R_j^S$  and  $R_j^L$  as model parameters in order to reproduce the experimentally observed STM images, the method provides essential information on the scattered electronic states and scattering mechanisms; however, it is not suitable to directly relate the

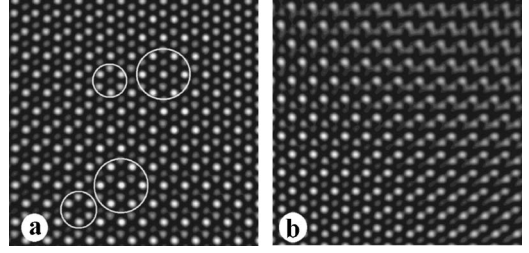


FIG. 3. Calculated spatial distributions of electron density  $|\psi(\vec{r})|^2$  according to Eq. (2). (a) Appropriate values of reflection amplitudes have been fitted to reproduce the experimentally observed coexisting interference patterns ( $V=0.1$  eV,  $\alpha=0.25$ ). (b) The resulting interference patterns of the same region sensitively changes by varying the applied bias potential ( $V=0.2$  eV,  $\alpha=0.25$ ).

observed long-range interference patterns to the atomic structure of the defects.

Because the geometry of the STM tip and the tip-tube distance cannot be directly inferred from the STM measurements, it is not possible to precisely calculate the magnitude of the Fermi-level shift. The magnitude of the Fermi-level shift due to the charging of the nanotube is controlled by the  $\alpha$  parameter in our model. However, the precise position of the Fermi level influences only the integration window, as can be seen from Fig. 2(c). The effect of integration over a set of scattered waves results in reduced oscillation amplitudes (reduced corrugation of the superstructures) of the electronic DOS due to wave-vector averaging; however, coexisting superstructure patterns can be reproduced even for no Fermi-level shift, i.e., for the  $\alpha=0$  parameter value.

The main conclusion resulting from comparing experimental and calculated STM images is that electronic states away from the  $K$  points involved in the scattering processes may give rise to position-dependent interference patterns in the following way: as we move away from  $K$  points, electronic states with wave vectors of different magnitude for forward- and backward-moving states get involved in the scattering process [Fig. 2(c)]. Wave functions characterized by wave vectors of different magnitude acquire different phase shifts as a function of the position relative to the defect site. The superposition of coherent wave functions with position-dependent relative phase leads to position-dependent interference conditions and consequently, to different coexisting superstructures.

It is worth mentioning that our model might be adaptable for the description of coexisting superstructures observed on graphite, with the observation that in the case of graphite for a given energy level all the states of the circular equienergetic surface can be involved in the scattering processes.

From Eqs. (1) and (2) it results that at a given position the arising complex interference patterns also depend on the applied bias potential in the STM configuration and the position of the Fermi surface, which is of particular importance in transport measurements, where the Fermi level of the CNTs can be easily controlled by the applied gate voltage. Figure 3 illustrates how defect sites in carbon nanotubes can act as tunable scattering centers for electrons and how the phenomena is perceptible by STM. Experimental indications of bias-dependent STM images of nanotube bend junctions

were provided by Odom *et al.*, who recorded STM images on bundles of SWCNT kink junctions. Images taken at different bias voltages at the bend region revealed different long-range electronic features.<sup>39</sup>

Transport measurements provide further experimental evidence of Fermi-energy-tunable behavior of individual defects in nanotubes.<sup>6</sup> Molecular electronic devices operating on this principle have already been built and constitute a novel class of electronic devices making use of quantum coherence.<sup>6,38</sup>

It is also expected that similar surface electron density oscillations significantly affect adsorbate structures, dynamics, and chemistry.<sup>40</sup> By varying the Fermi surface of the sample one should be able to tune the electron density distribution patterns and possibly influence the adsorption process.

#### IV. CONCLUSIONS

To summarize, we used STM to study defect-scattered electronic states, of particular importance from the point of

view of nanoelectronic devices, via long-range interference effects occurring due to the presence of defects in carbon nanotubes. We propose an interference model which can successfully reproduce coexisting superstructure patterns by considering electronic states away from the band crossing points involved in the scattering processes. The model was applied in the interpretation of position-dependent complex interference patterns revealed by atomic resolution STM measurements performed in the junction region of a MWCNT bend junction. Our results also shed some light on how Fermi-energy-tunable scattering processes take place in defective carbon nanotubes.

#### ACKNOWLEDGMENTS

This work was partly funded by OTKA Grant No. T 043685 in Hungary and partly by the IUAP program P5/01 “Quantum Size Effects in Nanostructured Materials” of the Belgian Science Policy Programming. The work in Romania was supported by the Sapientia Research Program Institute through Grant No. 1140/2004.

\*Email address: tapaszto@mfa.kfki.hu

- <sup>1</sup>S. Iijima, *Nature (London)* **354**, 56 (1991).
- <sup>2</sup>R. Saito, M. Fujita, G. Dresselhaus, and M. S. Dresselhaus, *Appl. Phys. Lett.* **60**, 2204 (1992).
- <sup>3</sup>Z. Yao, H. W. Ch. Postma, L. Balents, and C. Dekker, *Nature (London)* **402**, 273 (1999).
- <sup>4</sup>D. Bozovic, M. Bockrath, J. H. Hafner, C. M. Lieber, H. Park, and M. Tinkham, *Appl. Phys. Lett.* **78**, 3693 (2001).
- <sup>5</sup>D. Tekleab, R. Czerw, D. L. Carroll, and P. M. Ajayan, *Appl. Phys. Lett.* **76**, 3594 (2000).
- <sup>6</sup>M. Bockrath, W. Liang, D. Bozovic, J. H. Hafner, C. M. Lieber, M. Tinkham, and H. Park, *Science* **291**, 283 (2001).
- <sup>7</sup>J. W. Park, J. Kim, J. O. Lee, K. C. Kang, J. J. Kim, and K. H. Yoo, *Appl. Phys. Lett.* **80**, 133 (2002).
- <sup>8</sup>J. Kong, E. Yenilmez, T. W. Tombler, W. Kim, H. J. Dai, R. B. Laughlin, L. Liu, C. S. Jayanthi, and S. Y. Wu, *Phys. Rev. Lett.* **87**, 106801 (2001).
- <sup>9</sup>M. Ouyang, J. L. Huang, and C. M. Lieber, *Phys. Rev. Lett.* **88**, 066804 (2002).
- <sup>10</sup>M. F. Crommie, C. P. Lutz, and D. M. Eigler, *Nature (London)* **363**, 524 (1993).
- <sup>11</sup>A. Depuydt, C. Van Haesendonck, N. S. Maslova, V. I. Panov, S. V. Savinov, and P. I. Arseev, *Phys. Rev. B* **60**, 2619 (1999).
- <sup>12</sup>J. Xhie, K. Sattler, U. Muller, N. Venkateswaran, and G. Raina, *Phys. Rev. B* **43**, 8917 (1991).
- <sup>13</sup>W. Clauss, D. J. Bergeron, M. Freitag, C. L. Kane, E. J. Mele, and A. T. Johnson, *Europhys. Lett.* **47**, 601 (1999).
- <sup>14</sup>A. Hassanien, M. Tokumoto, P. Umek, D. Mihailovic, and A. Mrzel, *Appl. Phys. Lett.* **78**, 808 (2001).
- <sup>15</sup>M. Ishigami, H. J. Choi, S. Aloni, S. G. Louie, M. L. Cohen, and A. Zettl, *Phys. Rev. Lett.* **93**, 196803 (2004).
- <sup>16</sup>Z. Osváth, G. Vértésy, L. Tapasztó, F. Wéber, Z. E. Horváth, J. Gyulai, and L. P. Biró, *Phys. Rev. B* **72**, 045429 (2005).
- <sup>17</sup>P. Ruffieux, O. Gröning, P. Schwaller, L. Sclapbach, and P. Gröning, *Phys. Rev. Lett.* **84**, 4910 (2000).
- <sup>18</sup>P. Ruffieux, M. Melle-Franco, O. Groning, M. Biemann, F. Zerbetto, and P. Groning, *Phys. Rev. B* **71**, 153403 (2005).
- <sup>19</sup>H. A. Mizes and J. S. Foster, *Science* **244**, 559 (1989).
- <sup>20</sup>G. M. Shedd and P. E. Russell, *Surf. Sci.* **266**, 259 (1992).
- <sup>21</sup>N. Takeuchi, J. Valenzuela-Benavides, and L. Morales de la Garza, *Surf. Sci.* **380**, 190 (1997).
- <sup>22</sup>K. F. Kelly, D. Sarkar, G. D. Hale, S. J. Oldenburg, and N. J. Halas, *Science* **273**, 1371 (1996).
- <sup>23</sup>S. G. Lemay, J. W. Janssen, M. van den Hout, M. Moij, M. J. Bronikowski, P. A. Willis, R. E. Smalley, L. P. Kouwenhoven, and C. Dekker, *Nature (London)* **412**, 617 (2001).
- <sup>24</sup>L. C. Venema, J. W. G. Wildoer, J. W. Janssen, S. J. Tans, H. Tuinstra, L. P. Kouwenhoven, and C. Dekker, *Science* **283**, 52 (1999).
- <sup>25</sup>L. Tapasztó, K. Kertész, Z. Vértésy, Z. E. Horváth, A. A. Kóos, Z. Osváth, Zs. Sárközi, Al. Darabont, and L. P. Biró, *Carbon* **43**, 790 (2005).
- <sup>26</sup>W. Qian, T. Liu, F. Wei, Z. Wang, G. Luo, H. Yu, and Z. Li, *Carbon* **41**, 2613 (2003).
- <sup>27</sup>J. Han, M. P. Anantram, R. L. Jaffe, J. Kong, and H. Dai, *Phys. Rev. B* **57**, 14983 (1998).
- <sup>28</sup>L. P. Biró, J. Gyulai, Ph. Lambin, J. B. Nagy, S. Lazarescu, G. Márk, A. Fonseca, P. R. Surján, Zs. Szekeres, P. Thiry, and A. A. Lucas, *Carbon* **36**, 689 (1998).
- <sup>29</sup>J. I. Paredes, M. Burghard, A. Martinez-Alonso, and J. M. D. Tascon, *Appl. Phys. A* **80**, 675 (2005).
- <sup>30</sup>J. Tersoff and D. R. Hamann, *Phys. Rev. B* **31**, 805 (1985).
- <sup>31</sup>C. L. Kane and E. J. Mele, *Phys. Rev. B* **59**, R12759 (1999).
- <sup>32</sup>C. T. White and T. N. Todorov, *Nature (London)* **393**, 240 (1998).
- <sup>33</sup>L. C. Venema, J. W. Janssen, M. R. Buitelaar, J. W. G. Wildoer, S. G. Lemay, L. P. Kouwenhoven, and C. Dekker, *Phys. Rev. B* **62**, 5238 (2000).

- <sup>34</sup>L. Duclaux, *Carbon* **40**, 1751 (2005).
- <sup>35</sup>A. Bachtold, P. Hadley, T. Nakanishi, and C. Dekker, *Science* **294**, 1317 (2001).
- <sup>36</sup>P. Keblinski, S. K. Nayak, P. Zapol, and P. M. Ajayan, *Phys. Rev. Lett.* **89**, 255503 (2002).
- <sup>37</sup>A. Zazunov, D. Feinberg, and T. Martin, *Phys. Rev. B* **73**, 115405 (2006).
- <sup>38</sup>W. Liang, M. Bockrath, D. Bozovic, J. H. Hafner, M. Tinkham, and H. Park, *Nature (London)* **411**, 665 (2001).
- <sup>39</sup>T. W. Odom, J. L. Huang, P. Kim, and C. M. Lieber, *J. Phys. Chem. B* **104**, 2794 (2000).
- <sup>40</sup>S. A. Curran, A. V. Ellis, A. Vijayaraghavan, and P. M. Ajayan, *J. Chem. Phys.* **120**, 4886 (2004).